Available online at www.sciencedirect.com
ScienceDirect
Journal of Computational Physics 227 (2007) 79–99
JOURNAL OF COMPUTATIONAL PHYSICS
www.elsevier.com/locate/jcp

A solution for the odd–even decoupling problem in pressure-correction algorithms for variable density flows

Pieter Rauwoens *, Jan Vierendeels, Bart Merci [1]

Ghent University – UGent, Department of Flow, Heat and Combustion Mechanics, Sint-Pietersnieuwstraat 41, B-9000 Ghent, Belgium

Received 25 January 2007; received in revised form 17 July 2007; accepted 17 July 2007
Available online 31 July 2007

Abstract

When the Navier–Stokes equations are solved on a colocated mesh, a spurious mode for the pressure can appear if no special attention is paid to the discretization of the pressure. This pressure mode can be suppressed by a pressure-weighted interpolation formula for the mass flux over a cell-face. In this paper, a similar cure is presented in the framework of pressure-correction methods in variable density flow. Special attention is given to the solvability condition for the resulting Poisson-like equation for the pressure. It consists of two remedies: a correction term for the cell-face velocity is introduced and the stencil for the discrete Laplacian is compacted. We finally show the applicability of the method on general curvilinear coordinate systems in three dimensions.

MSC: 65N12; 65N22; 76D05; 76M12; 76R99

Keywords: Solvability condition; Odd–even decoupling; Pressure-correction; Variable density flow; Spurious mode

1. Introduction

It is well-known [13] that discretization of the partial differential flow equations on a mesh with colocated variables, which means that the local state variables are stored at the same position, can give rise to a *spurious mode* (a π-wave) for the pressure, when the cell-face velocities are linearly interpolated between the neighbouring nodes without pressure stabilization and when the pressure term in the momentum equations is approximated by central differencing. This mode is not seen by the discretized equations, and results in a solution without physical meaning.

A solution for this problem is a *staggered* treatment of the variables [13]. Variants of the pressure-correction scheme of this type are the MAC (Marker-And-Cell) [7] and the SIMPLE (Semi-Implicit Method for

* Corresponding author.
E-mail addresses: Pieter.Rauwoens@UGent.be (P. Rauwoens), Jan.Vierendeels@UGent.be (J. Vierendeels), Bart.Merci@UGent.be (B. Merci).
[1] Postdoctoral Fellow of the *Fund of Scientific Research – Flanders (Belgium) (FWO-Vlaanderen)*.

0021-9991/$ - see front matter © 2007 Elsevier Inc. All rights reserved.
doi:10.1016/j.jcp.2007.07.010

Pressure-Linked Equations) [11] methods. If rectangular grids are used, the choice of a staggered grid arrangement is the most natural choice for a straightforward discretization of the governing equations. However, this approach is not comfortable, especially in a three-dimensional environment making use of body-fitted grids [10]. In these more general cases there are practical advantages to use grids with colocated arrangements. Although convenient, a major drawback is found in the complication of the algorithms to filter out spurious modes. This problem can then be resolved by using special flux-splitting schemes [5] or pressure weighted interpolation (PWI) methods, as first introduced in [15]. Other propositions, concerning pressure weighted velocity interpolation or pressure gradient interpolation were made in [2,3,18] for low Mach number flows or in [6,9] for flows at all speeds. Unfortunately, in time-accurate solutions of variable density flows, special requirements of system solvability are not unconditionally fulfilled by these propositions. We come back to this point later in the paper.

In this paper we rigorously derive a solution formalism for solving the odd–even decoupling problem in the framework of pressure-correction algorithms for variable density flows. In the next section the pressure correction scheme applied to the low Mach continuity, momentum and energy equations, is given without a remedy for odd–even decoupling. Emphasis is put on the solvability condition of the resulting Poisson equation for the pressure and the problem of the spurious mode is further elaborated. Section 3 describes the cure for the odd–even decoupling including variable density. It consists of two remedies: a correction term for the cell-face velocity, similar to [15], is introduced and the stencil for the discrete Laplacian in the equation for pressure is compacted. Section 4 shows the applicability of the method on general curvilinear coordinate systems in three dimensions. Section 5 compares the present cure with other remedies for odd–even decoupling in the literature. In Section 6, finally, the method is applied to a two-dimensional thermally driven cavity with large temperature differences.

2. Problem setting

2.1. Governing equations

In this paper, the non-dimensional Navier–Stokes equations are considered in the limit of zero Mach number [12]

$$p_0 = p_0(t), \tag{1}$$

$$\frac{\partial \rho}{\partial t} + \frac{\partial(\rho u_i)}{\partial x_i} = 0, \tag{2}$$

$$\frac{\partial(\rho u_j)}{\partial t} + \frac{\partial(\rho u_i u_j)}{\partial x_i} = -\frac{\partial p_2}{\partial x_j} + \frac{1}{Re_\infty}\frac{\partial \tau_{ij}}{\partial x_i} + \frac{1}{Fr_\infty^2}\rho\delta_{j3}, \tag{3}$$

$$\frac{\gamma}{\gamma-1}\rho\left[\frac{\partial T}{\partial t} + u_i\frac{\partial T}{\partial x_i}\right] - \frac{\mathrm{d}p_0}{\mathrm{d}t} = \frac{\gamma}{(\gamma-1)Re_\infty Pr_\infty}\frac{\partial}{\partial x_i}\left(\kappa\frac{\partial T}{\partial x_i}\right), \tag{4}$$

with the zeroth-order equation of state

$$p_0 = \rho T. \tag{5}$$

In these equations, ρ denotes the local density, u_i the component of the velocity vector in the i-direction, T the temperature, κ the heat conduction coefficient and $\gamma = c_p/c_v$ the specific heat ratio. t is the time coordinate and x_i are the spatial coordinates for each dimension. Without lack of generality, we assume that the gravity is aligned with the third axis. The pressure p is expanded into a thermodynamic and a kinematic part: $p = p_0 + \widetilde{M}_\infty^2 p_2$. Unless we are dealing with enclosed systems, the thermodynamic pressure is assumed constant in space and time.

The non-dimensional parameters are

$$\widetilde{M}_\infty = \frac{u_\infty}{\sqrt{p_\infty/\rho_\infty}}, \quad Re_\infty = \frac{\rho_\infty u_\infty L}{\mu_\infty}, \quad Fr_\infty = \frac{u_\infty}{\sqrt{gL}}, \quad Pr_\infty = \frac{c_p\mu_\infty}{\kappa_\infty}, \tag{6}$$

where the subscript ∞ denotes reference values, L a reference length and g the gravitational constant.

For cases involving natural convection, the reference velocity is chosen as $u_\infty = \kappa/\rho L c_p$ [1], so that $Re_\infty Pr_\infty = 1$. Hence the non-dimensional momentum equation takes the form

$$\frac{\partial(\rho u_j)}{\partial t} + \frac{\partial(\rho u_i u_j)}{\partial x_i} = -\frac{\partial p_2}{\partial x_j} + Pr_\infty \frac{\partial \tau_{ij}}{\partial x_i} + \frac{Ra_\infty Pr_\infty}{2\epsilon}\rho\delta_{j3} \tag{7}$$

with $Ra_\infty = \frac{Re_\infty^2 Pr_\infty 2\epsilon}{Fr_\infty^2}$ and ϵ a non-dimensional temperature difference, defined in Section 6.1.

2.2. Pressure-correction algorithm

The pressure-correction algorithm is completely described in [14] ('Constraint-Based Pressure-Correction in revised form'). We briefly repeat the most important features for a 1D case in order to reveal the odd–even decoupling and its solution. First, Eq. (4) is rewritten in terms of density, using equation of state (5) and continuity Eq. (2)

$$\frac{\partial \rho}{\partial t} + u_i \frac{\partial \rho}{\partial x_i} = \frac{\rho}{\gamma p_0}\frac{\mathrm{d}p_0}{\mathrm{d}t} - \rho\frac{\partial q_i}{\partial x_i} \tag{8}$$

with $q_i = \frac{\kappa}{Re_\infty Pr_\infty}\frac{\partial(1/\rho)}{\partial x_i}$.

The constraint on the velocity field is then derived from a combination of (2) and (8)

$$-\frac{\partial \rho u}{\partial x} + u\frac{\partial \rho}{\partial x} = -\rho\frac{\partial q}{\partial x}. \tag{9}$$

The discrete algorithm consists of the different substeps, given below.

2.2.1. Density stepping

$$\frac{\rho_i^{n+1} - \rho_i^n}{\Delta t} = -\frac{u_{i+\frac{1}{2}}^n \rho_{\mathrm{R}}^n - u_{i-\frac{1}{2}}^n \rho_{\mathrm{L}}^n}{\Delta x}. \tag{10}$$

The L and R subscripts indicate extrapolated values at the left and right surface of the control volume respectively. The subscript $i+\frac{1}{2}$ refers to a simple arithmetic mean: $u_{i+\frac{1}{2}} = \frac{u_i + u_{i+1}}{2}$.

2.2.2. Velocity predictor

The equations are solved here by means of a projection method, i.e. the intermediate state for the velocity is determined by removing the pressure from Eq. (3). The prediction of the velocity u^* is then found from

$$\frac{(\rho^{n+1}u^*)_i - (\rho u)_i^n}{\Delta t} = -\frac{u_{i+\frac{1}{2}}^n (\rho u)_{\mathrm{R}}^n - u_{i-\frac{1}{2}}^n (\rho u)_{\mathrm{L}}^n}{\Delta x} + \frac{1}{Re_\infty}\left(\frac{\partial \tau_{ij}}{\partial x_i}\right)^n + \frac{\rho_i}{Fr_\infty^2}. \tag{11}$$

The specific discretization of the viscous fluxes is of no importance and the gravitational force is assumed to be aligned with the considered direction of the 1D problem.

2.2.3. Velocity constraint

$$-\frac{\rho_{\mathrm{R}}^{n+1} u_{i+\frac{1}{2}}^{n+1} - \rho_{\mathrm{L}}^{n+1} u_{i-\frac{1}{2}}^{n+1}}{\Delta x} + u_i^{n+1}\frac{\rho_{\mathrm{R}}^{n+1} - \rho_{\mathrm{L}}^{n+1}}{\Delta x} = -\frac{\rho^{n+1}}{Re_\infty Pr_\infty}\frac{\partial}{\partial x}\left(\kappa\frac{\partial}{\partial x}\left(\frac{1}{\rho^{n+1}}\right)\right) + \frac{\rho}{\gamma p_0}\frac{\mathrm{d}p_0}{\mathrm{d}t}^{n+1}. \tag{12}$$

Inserting $u_i^{n+1} = u_i^* - \Delta t\frac{p_{i+1}^{n+1} - p_{i-1}^{n+1}}{2\rho_i \Delta x}$ in the last equation results in a Poisson-like equation for the pressure. The discretization of the conductive fluxes will be defined below.

2.3. Example: Conduction in a 1D adiabatic channel

Consider the conduction of a density jump in an adiabatic 1D channel with constant cross-section. The channel is closed at both ends, so that wall boundary conditions apply. For this case, the non-dimensional flow Eqs. (2), (3) and (8) become

$$\frac{\partial \rho}{\partial t} + \frac{\partial \rho u}{\partial x} = 0, \tag{13}$$

$$\frac{\partial \rho u}{\partial t} + \frac{\partial \rho u^2}{\partial x} + \frac{\partial p_2}{\partial x} = 0, \tag{14}$$

$$\frac{\partial \rho}{\partial t} + u\frac{\partial \rho}{\partial x} = -\rho\frac{\partial q}{\partial x}. \tag{15}$$

Note that the thermodynamic pressure p_0 does not change in time in an adiabatic environment.

The initial conditions are

$$\begin{aligned} \rho(t_0) &= \rho_0 + \rho_1 H(x - x_0), \\ u(t_0) &= 0 \end{aligned} \tag{16}$$

with $H(x)$ the heaviside function.

The equations are discretized using first-order velocity upwinding for the convective terms and second-order central discretization for the conductive and pressure term. For every node a Poisson-like equation for the pressure can be derived, resulting formally in the matrix expression

$$LP = B, \tag{17}$$

with L the discrete Laplacian-like operator, $P = [p_1 \quad p_2 \quad \cdots \quad p_N]^{\mathrm{T}}$ the pressure vector and B the right hand side, containing the predicted velocity values and the conductive terms. Note that in case of a pressure-correction method, in (17) we would have P' instead of P, the vector of pressure corrections.

The system is singular and contains a nullspace of dimension 2, for which $LP = 0$. Indeed, two spurious modes exist: the hydrostatic pressure field $P_{\mathrm{H}} = [1 \quad 1 \quad \cdots \quad 1]^{\mathrm{T}}$ and the π-wave $P_\pi = [1 \quad -1 \quad \cdots \quad (-1)^{N+1}]^{\mathrm{T}}$.

We can perform the same analysis for the transpose of the operator L, resulting again in a nullspace of dimension 2, based on 2 vectors R_{H} and R_π, for which $R^{\mathrm{T}}L = 0$. The exact expressions for these vectors cannot easily be determined. For the set of discretized equations in the pressure-correction step to be solvable, the RHS of the equation has to fulfill certain conditions

$$\begin{aligned} R_{\mathrm{H}}^{\mathrm{T}} LP &= R_{\mathrm{H}}^{\mathrm{T}} B = 0, \\ R_\pi^{\mathrm{T}} LP &= R_\pi^{\mathrm{T}} B = 0. \end{aligned} \tag{18}$$

It is more instructive to consider these restrictions at the level of the constraining equation for the velocity, from which the Poisson-like equation is derived. For an internal node, we can write (9) in a semi-discretized manner

$$-\frac{\rho_{\mathrm{R}} u_{i+\frac{1}{2}} - \rho_{\mathrm{L}} u_{i-\frac{1}{2}}}{\Delta x} + u_i \frac{\rho_{\mathrm{R}} - \rho_{\mathrm{L}}}{\Delta x} = -\frac{\rho}{Re_\infty Pr_\infty}\frac{\partial}{\partial x}\left(\kappa \frac{\partial}{\partial x}\left(\frac{1}{\rho}\right)\right), \tag{19}$$

where all variables are evaluated at time level $n+1$. If the RHS is discretized in the same manner as the LHS, system (17) is solvable (see also Appendix A) and the fully discretized equation becomes

$$-\frac{\rho_{\mathrm{R}} u_{i+\frac{1}{2}} - \rho_{\mathrm{L}} u_{i-\frac{1}{2}}}{\Delta x} + u_i \frac{\rho_{\mathrm{R}} - \rho_{\mathrm{L}}}{\Delta x} = -\frac{\rho_{\mathrm{R}} q_{i+\frac{1}{2}} - \rho_{\mathrm{L}} q_{i-\frac{1}{2}}}{\Delta x} + q_i \frac{\rho_{\mathrm{R}} - \rho_{\mathrm{L}}}{\Delta x} \tag{20}$$

with

$$q_i = \frac{\kappa_i}{Re_\infty Pr_\infty} \frac{\frac{1}{\rho_{i+1}} - \frac{1}{\rho_{i-1}}}{2\Delta x} \tag{21}$$

and

$$q_{i+\frac{1}{2}} = \frac{q_i + q_{i+1}}{2}. \tag{22}$$

For the system to be solvable, the important observation is thus that the conductive fluxes must be calculated at the nodes and interpolated towards the cell faces. Since these terms are evaluated centrally, a π-wave for the density is not noticed and can consequently increase without limitation. As a result, the spurious pressure

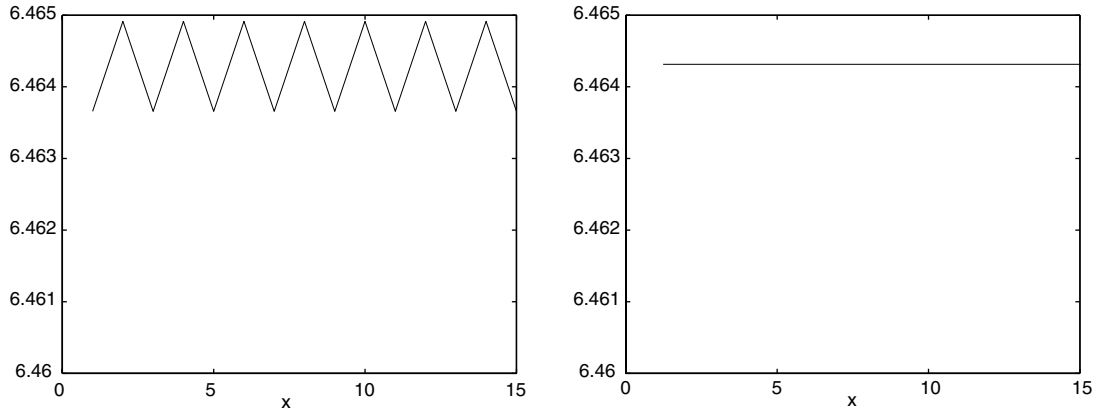

Fig. 1. Density plot of the converged solution for the conductive heat transfer in a 1D adiabatic channel, discretized in 15 points. Initial conditions (16) apply with $\rho_0 = 1$, $\rho_1 = 10$, $x_0 = 7$. A spurious mode for the density appears (left), compared to the exact solution (right).

wave gives rise to unphysical results not only for the pressure, but also for other variables, such as the density, as shown in Fig. 1.

2.4. Solvability condition

From the above example, it is clear that any cure for the odd–even decoupling problem, should comply with the solvability conditions of the Poisson-like pressure equation. So, a good remedy for the odd–even decoupling problem does not only remove the spurious mode P_π from the solution, but also guarantees that the resulting system is solvable. Indeed, although the spurious mode P_π were to be removed form the solution of example 1, the resulting system is still singular with a nullspace of dimension 1, and one condition for the RHS remains from (18)

$$R_{\mathrm{H}}^{\mathrm{T}} L P = R_{\mathrm{H}}^{\mathrm{T}} B = 0. \tag{23}$$

In general, this condition is not fulfilled if one does not apply the propositions made by e.g. [2,3,15] in a rigorous way, i.e. by considering the first principles of these propositions in the special case of a variable-density pressure-correction or pressure-projection method.

In addition to the solvability requirement, we prefer a discrete Laplacian of the pressure field, that is easily solvable by an iterative method, i.e. a Laplacian with a compact stencil.

3. Adjusted algorithm

We consider Eqs. (2), (3) and (8). The basic algorithm is the same as described in Section 2.2, discretized on a colocated mesh. However, to cure the odd–even decoupling, certain equations are assumed to be solved in a staggered way. Note that we use the assumption only to derive the algorithm, suitable for a colocated mesh approach. As a result of the staggered approach assumption, extra terms appear in the discretization. In this section, we restrict ourselves to a one-dimensional uniform mesh with grid spacing Δx. In Section 4, the reasoning is generalized to general curvilinear meshes in three dimensions.

We introduce notations $\tilde{\phi}$ and $\bar{\phi}$. The former is defined on the cell face and is calculated as the arithmetic mean of the neighbouring node values; the latter is defined in the node and is calculated as the mean of the neighbouring face values

$$\tilde{\phi}_{i+\frac{1}{2}} = \frac{\phi_i + \phi_{i+1}}{2}, \quad \bar{\phi}_i = \frac{\phi_{i-\frac{1}{2}} + \phi_{i+\frac{1}{2}}}{2}. \tag{24}$$

The algorithm is first presented as such, after which the subsequent substeps, including the derivation of the correction term, are explained in greater detail, starting from known values at time level n.

3.1. Summary

Given an initial density field ρ_i^0, thermodynamic pressure p_0^0 and an initial velocity field u_i^0 (and kinematic pressure field p_i^0), satisfying the velocity constraint, the cured pressure-correction scheme consists of the substeps shown in the flowchart of Fig. 2. The correction for the cell-face velocities $\hat{\varepsilon}$ considers $\frac{\nabla p}{\rho}$ as an entity and is used in the convective terms of continuity and momentum equation. The pressure follows from a Poisson-like equation, originating from a combination of the equations of continuity and temperature.

3.2. Density stepping

For now, we do not yet specify how to determine ρ_i^{n+1} and consider this quantity as known. The exact way of calculating ρ_i^{n+1} can be found under Section 3.6.

3.3. Velocity predictor

The prediction of the velocity u_i^* is done in the same way as (11), now using the interpolation notation

$$\frac{(\rho^{n+1}u^*)_i - (\rho u)_i^n}{\Delta t} = -\frac{\tilde{u}^n_{i+\frac{1}{2}}(\rho u)^n_{\mathrm{R}} - \tilde{u}^n_{i-\frac{1}{2}}(\rho u)^n_{\mathrm{L}}}{\Delta x} + \frac{1}{Re_\infty}\left(\frac{\partial \tau_{ij}}{\partial x_i}\right)^n. \tag{25}$$

Again, the discretization details of the viscous term are of no importance.

3.4. Velocity corrector

The velocity at the new time level is now calculated using the predicted velocity field, and the correction from the pressure term. Since the pressure in colocated formulation gives rise to spurious modes in the solution, the relationship between pressure and velocity is expressed here as if the corrector step were solved on a staggered mesh. Hence, the following staggered momentum equations are thought to be solved:

$$\frac{u^{n+1}_{i+\frac{1}{2}} - \tilde{u}^*_{i+\frac{1}{2}}}{\Delta t} = -\frac{1}{\tilde{\rho}^{n+1}_{i+\frac{1}{2}}}\frac{p^{n+1}_{i+1} - p^{n+1}_i}{\Delta x}, \tag{26}$$

$$\frac{u^{n+1}_{i-\frac{1}{2}} - \tilde{u}^*_{i-\frac{1}{2}}}{\Delta t} = -\frac{1}{\tilde{\rho}^{n+1}_{i-\frac{1}{2}}}\frac{p^{n+1}_{i} - p^{n+1}_{i-1}}{\Delta x}. \tag{27}$$

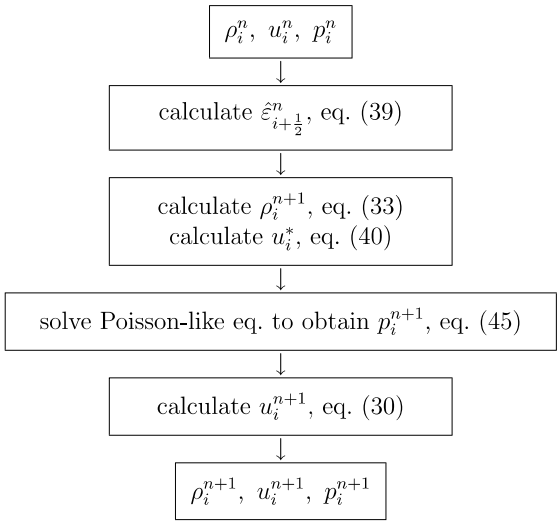

Fig. 2. Summary of the pressure-correction algorithm, cured for odd–even decoupling.

Combination of (26) and (27) gives a colocated formulation

$$\bar{u}_i^{n+1} - \tilde{\bar{u}}_i^* = -\frac{\Delta t}{2\Delta x}\left[\frac{p_{i+1}^{n+1} - p_i^{n+1}}{\tilde{\rho}_{i+\frac{1}{2}}^{n+1}} + \frac{p_i^{n+1} - p_{i-1}^{n+1}}{\tilde{\rho}_{i-\frac{1}{2}}^{n+1}}\right]. \tag{28}$$

We write the last equation in a more compact form

$$\bar{u}_i^{n+1} - \tilde{\bar{u}}_i^* = -\frac{\Delta t}{2}\left[\frac{\nabla p}{\tilde{\rho}}\bigg|_{i+\frac{1}{2}}^{n+1} + \frac{\nabla p}{\tilde{\rho}}\bigg|_{i-\frac{1}{2}}^{n+1}\right] = -\Delta t\overline{\frac{\nabla p}{\tilde{\rho}}}\bigg|_i^{n+1}. \tag{29}$$

However, a problem arises if we use this expression each time step. The calculated velocity field would then become too smooth because of the averaging of u^*. Indeed, on a colocated mesh, the velocity is normally calculated from

$$u_i^{n+1} - u_i^* = -\Delta t\overline{\frac{\nabla p}{\tilde{\rho}}}\bigg|_i^{n+1} \tag{30}$$

with no averages in the LHS. The relationship between u_i^{n+1} and $\bar{u}_i^{n+1}$ is determined from Eqs. (30) and (29)

$$u_i^{n+1} = \bar{u}_i^{n+1} + (u_i^* - \tilde{\bar{u}}_i^*). \tag{31}$$

3.5. Pressure correction equation

The corrected velocity u_i^{n+1} can be determined from (30) if the pressure field is known. The pressure is calculated from the pressure correction equation, following from a constraining equation on the velocity field. The velocity field has to satisfy the continuity equation (13), with (provisionally) an imposed change in density $\frac{\partial\rho}{\partial t} = \frac{\rho^{n+2}-\rho^{n+1}}{\Delta t}$

$$\frac{\partial\rho}{\partial t}\bigg|_i = -\frac{\rho_{\mathrm{R}}^{n+1}u_{i+\frac{1}{2}}^{n+1} - \rho_{\mathrm{L}}^{n+1}u_{i-\frac{1}{2}}^{n+1}}{\Delta x} = -\frac{\rho_{\mathrm{R}}^{n+1}\tilde{u}_{i+\frac{1}{2}}^* - \rho_{\mathrm{L}}^{n+1}\tilde{u}_{i-\frac{1}{2}}^*}{\Delta x} + \frac{\Delta t}{\Delta x}\left[\rho_{\mathrm{R}}^{n+1}\frac{\nabla p}{\tilde{\rho}}\bigg|_{i+\frac{1}{2}}^{n+1} - \rho_{\mathrm{L}}^{n+1}\frac{\nabla p}{\tilde{\rho}}\bigg|_{i-\frac{1}{2}}^{n+1}\right], \tag{32}$$

where the last step uses the staggered momentum equations (26) and (27). Eq. (32) is a Poisson equation for the pressure, where the spurious pressure mode P_π no longer is part of the solution of the system. Using the staggered equations thus eliminates the spurious mode.

3.6. Density stepping (completed)

In case of the pressure-correction algorithm in Section 2.2, the density is determined from the conservation equation of mass. The value obtained for $\frac{\partial\rho}{\partial t} = \frac{\rho^{n+2}-\rho^{n+1}}{\Delta t}$ must be identical to (32) but is calculated using colocated variables

$$\frac{\partial\rho}{\partial t}\bigg|_i = -\frac{\rho_{\mathrm{R}}^{n+1}\underline{u}_{i+\frac{1}{2}}^{n+1} - \rho_{\mathrm{L}}^{n+1}\underline{u}_{i-\frac{1}{2}}^{n+1}}{\Delta x} \tag{33}$$

with $\underline{u}$ a corrected interpolation, given by

$$\underline{u}_{i+\frac{1}{2}} = \tilde{\bar{u}}_{i+\frac{1}{2}} + \varepsilon_{i+\frac{1}{2}}. \tag{34}$$

Equalization of (32) and (33) yields, for the flux at the right cell face

$$\rho_{\mathrm{R}}^{n+1}\tilde{u}_{i+\frac{1}{2}}^* - \Delta t\rho_{\mathrm{R}}^{n+1}\frac{\nabla p}{\tilde{\rho}}\bigg|_{i+\frac{1}{2}}^{n+1} = \rho_{\mathrm{R}}^{n+1}\underline{u}_{i+\frac{1}{2}}^{n+1}. \tag{35}$$

For the corrector equation (28), we can further elaborate the previous expression

$$\Longleftrightarrow \tilde{u}^{*}_{i+\frac{1}{2}} - \Delta t \frac{\nabla p}{\tilde{\rho}}\bigg|^{n+1}_{i+\frac{1}{2}} = \tilde{\bar{u}}^{n+1}_{i+\frac{1}{2}} + \varepsilon^{n+1}_{i+\frac{1}{2}} = \frac{\bar{u}^{n+1}_{i} + \bar{u}^{n+1}_{i+1}}{2} + \varepsilon^{n+1}_{i+\frac{1}{2}}$$

$$= \frac{\tilde{\bar{u}}^{*}_{i} + \tilde{\bar{u}}^{*}_{i+1}}{2} - \frac{\Delta t}{2}\left[\frac{\overline{\nabla p}}{\tilde{\rho}}\bigg|^{n+1}_{i} + \frac{\overline{\nabla p}}{\tilde{\rho}}\bigg|^{n+1}_{i+1}\right] + \varepsilon^{n+1}_{i+\frac{1}{2}} = \tilde{\tilde{u}}^{*}_{i+\frac{1}{2}} - \Delta t \frac{\widetilde{\overline{\nabla p}}}{\tilde{\rho}}\bigg|^{n+1}_{i+\frac{1}{2}} + \varepsilon^{n+1}_{i+\frac{1}{2}}, \tag{36}$$

from which the correction term follows:

$$\varepsilon^{n+1}_{i+\frac{1}{2}} = \left[\tilde{u}^{*}_{i+\frac{1}{2}} - \tilde{\tilde{u}}^{*}_{i+\frac{1}{2}}\right] - \Delta t \left[\frac{\nabla p}{\tilde{\rho}}\bigg|^{n+1}_{i+\frac{1}{2}} - \frac{\widetilde{\overline{\nabla p}}}{\tilde{\rho}}\bigg|^{n+1}_{i+\frac{1}{2}}\right]. \tag{37}$$

If we redefine the corrected interpolation (34) as

$$\underline{\phi}_{i+\frac{1}{2}} = \tilde{\phi}_{i+\frac{1}{2}} + \hat{\varepsilon}_{i+\frac{1}{2}} \tag{38}$$

for the corrector Eq. (30), the new correction term $\hat{\varepsilon}$ becomes

$$\hat{\varepsilon}^{n+1}_{i+\frac{1}{2}} = -\Delta t \left[\frac{\nabla p}{\tilde{\rho}}\bigg|^{n+1}_{i+\frac{1}{2}} - \frac{\widetilde{\overline{\nabla p}}}{\tilde{\rho}}\bigg|^{n+1}_{i+\frac{1}{2}}\right], \tag{39}$$

which is the analogue of expression (27) in [15].

For consistency, the same cell-face velocity interpolation is used in the velocity predictor step, so that (25) now becomes

$$\frac{(\rho^{n+1}u^{*})_i - (\rho u)^{n}_{i}}{\Delta t} = -\frac{\underline{u}^{n}_{i+\frac{1}{2}}(\rho u)^{n}_{\mathrm{R}} - \underline{u}^{n}_{i-\frac{1}{2}}(\rho u)^{n}_{\mathrm{L}}}{\Delta x} + \frac{1}{Re_{\infty}}\left(\frac{\partial \tau_{ij}}{\partial x_i}\right)^{n}. \tag{40}$$

3.7. Correction equation (completed)

Eq. (32) is now completed for the pressure field to be calculated. To fix thoughts, the abovementioned pressure-correction algorithm is considered, although other alternatives are possible as well [14]. The variation in time of density $\frac{\partial \rho}{\partial t}$ is obtained from the equation of temperature (15), discretized as

$$\frac{\partial \rho}{\partial t}\bigg|_i = -\bar{u}^{n+1}_{i}\frac{\rho^{n+1}_{\mathrm{R}} - \rho^{n+1}_{\mathrm{L}}}{\Delta x} - \rho\frac{\partial q}{\partial x} = \left[\tilde{\bar{u}}^{*}_{i} - \Delta t \frac{\overline{\nabla p}}{\tilde{\rho}}\bigg|^{n+1}_{i}\right]\frac{\rho^{n+1}_{\mathrm{R}} - \rho^{n+1}_{\mathrm{L}}}{\Delta x} - \rho\frac{\partial q}{\partial x}. \tag{41}$$

Elimination of $\frac{\partial \rho}{\partial t}$ from (41) and (32), results in the pressure Poisson-like equation

$$\frac{\rho^{n+1}_{\mathrm{R}} + \rho^{n+1}_{\mathrm{L}}}{2}\frac{\Delta t}{\Delta x}\left[\frac{\nabla p}{\tilde{\rho}}\bigg|^{n+1}_{i+\frac{1}{2}} - \frac{\nabla p}{\tilde{\rho}}\bigg|^{n+1}_{i-\frac{1}{2}}\right] = \frac{\rho^{n+1}_{\mathrm{R}} + \rho^{n+1}_{\mathrm{L}}}{2}\frac{\tilde{u}^{*}_{i+\frac{1}{2}} - \tilde{u}^{*}_{i-\frac{1}{2}}}{\Delta x} - \rho\frac{\partial q}{\partial x}. \tag{42}$$

This set of equations can again formally be written as (17), with L now a matrix with a nullspace of dimension 1 (the hydrostatic pressure field). We can perform the same analysis for the system to be solvable as in Example 2.3, resulting in a discretization of the conductive term under the form:

$$\rho\frac{\partial q}{\partial x} = \frac{\rho^{n+1}_{\mathrm{R}} + \rho^{n+1}_{\mathrm{L}}}{2}\frac{q^{n+1}_{i+\frac{1}{2}} - q^{n+1}_{i-\frac{1}{2}}}{\Delta x} \tag{43}$$

with

$$q^{n+1}_{i+\frac{1}{2}} = \frac{\kappa_i}{Re_{\infty}Pr_{\infty}}\frac{\frac{1}{\rho^{n+1}_{i+1}} - \frac{1}{\rho^{n+1}_{i}}}{\Delta x}. \tag{44}$$

Using (43), (42) is simplified to

$$\frac{\Delta t}{\Delta x}\left[\frac{\nabla p}{\tilde{\rho}}\bigg|_{i+\frac{1}{2}}^{n+1}-\frac{\nabla p}{\tilde{\rho}}\bigg|_{i-\frac{1}{2}}^{n+1}\right]=\frac{\tilde{u}_{i+\frac{1}{2}}^{*}-\tilde{u}_{i-\frac{1}{2}}^{*}}{\Delta x}-\frac{q_{i+\frac{1}{2}}^{n+1}-q_{i-\frac{1}{2}}^{n+1}}{\Delta x}. \tag{45}$$

Note that correction term (37), although apparent in the calculation of the density at the new time level, does not appear in the Poisson-like equation for the pressure. Hence, the continuity equation used to derive the constraint for the velocity, and thus the pressure Poisson-like equation, has a different formulation than the continuity equation used to predict the new density field.

Also note that Eq. (45) does not contain any upwind values. This is an advantage in terms of efficiency, since in general the sign of the velocity components at the new time level is not known. Thus, if upwind values appeared, the Laplacian operator would need to be evaluated every iteration per time step. Here, only one evaluation per time step is required.

4. Extension to general curvilinear coordinate systems in 3D

The extension of the previous approach towards three-dimensional cartesian equidistant meshes is straightforward. Application of the method on general structured grids is still possible by means of a rigourous deduction, based on the invariant formulation of the Navier–Stokes equations. In this formulation the physical domain is mapped onto a rectangular block (Fig. 3). Hence the curvilinear grid is mapped onto a cartesian equidistant grid, on which the above solution method can be applied. From now onwards, we use the notations corresponding to the mapping theory [10,16]. This implies that the coordinate indices are written in superscript.

4.1. Finite volume formulation in general coordinates

We note the Navier–Stokes equations in an invariant formulation, according to [10,16]. The equations on a cartesian grid are the following [14]:

$$\begin{aligned}&\frac{\partial \rho}{\partial t}+\frac{\partial(\rho u_i)}{\partial x^i}=0,\\&\left(\frac{\partial \rho u_j}{\partial t}\right)^{\diamondsuit}+\frac{\partial p}{\partial x^j}=0,\\&\frac{\partial \rho}{\partial t}+u_i\frac{\partial \rho}{\partial x^i}=\mathrm{Cond}(\rho)\end{aligned} \tag{46}$$

with

$$\mathrm{Cond}(\rho)=-\frac{\rho}{Re_\infty Pr_\infty}\frac{\partial}{\partial x^i}\left(\kappa\frac{\partial}{\partial x^i}\left(\frac{1}{\rho}\right)\right). \tag{47}$$

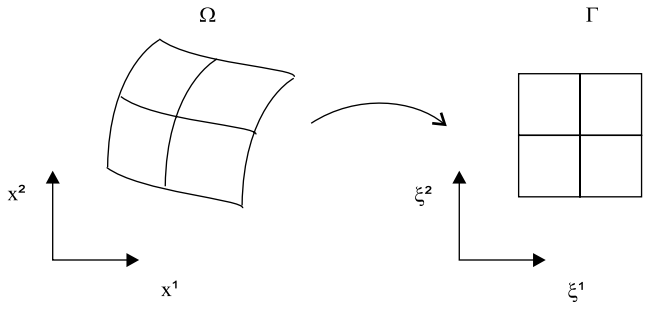

Fig. 3. Mapping of a physical domain Ω onto a rectangular block Γ.

The diamond ($\diamondsuit$) is introduced because the convective and diffusive transport in the momentum equation is not written, so that the update in time is done from state $(\rho u)^*$ to state $(\rho u)^{n+1}$

$$\left(\frac{\partial \rho u_j}{\partial t}\right) + \frac{\partial \rho u_i u_j}{\partial x^i} - \text{Visc} + \frac{\partial p}{\partial x^j} = 0$$
$$\Longleftrightarrow \left(\frac{\partial \rho u_j}{\partial t}\right)^* + \left(\frac{\partial \rho u_j}{\partial t}\right)^{\diamondsuit} + \frac{\partial \rho u_i u_j}{\partial x^i} - \text{Visc} + \frac{\partial p}{\partial x^j} = 0$$

with $\left(\frac{\partial \rho u_j}{\partial t}\right)^*$ following from the predictor step:

$$\left(\frac{\partial \rho u_j}{\partial t}\right)^* + \frac{\partial \rho u_i u_j}{\partial x^i} - \text{Visc} = 0.$$

Written in integral formulation the equations become

$$\begin{aligned}
&\iiint_\Omega \frac{\partial \rho}{\partial t}\,\mathrm{d}V + \iint_{\partial\Omega} \rho \boldsymbol{u}\cdot\boldsymbol{n}\,\mathrm{d}S = 0,\\
&\iiint_\Omega \left(\frac{\partial \rho \boldsymbol{u}}{\partial t}\right)^{\diamondsuit}\mathrm{d}V + \iint_{\partial\Omega} p\boldsymbol{n}\,\mathrm{d}S = 0,\\
&\iiint_\Omega \frac{\partial \rho}{\partial t}\,\mathrm{d}V + \iiint_\Omega \boldsymbol{u}\cdot\nabla\rho\,\mathrm{d}V = \iiint_\Omega \mathrm{Cond}(\rho)\,\mathrm{d}V.
\end{aligned} \tag{48}$$

The above equations are transformed to the coordinate system (ξ^1,ξ^2,ξ^3), with metric tensor

$$\begin{aligned}
&g_{\alpha\beta} = \frac{\partial x^k}{\partial \xi^\alpha}\frac{\partial x^k}{\partial \xi^\beta},\\
&g = \det(g_{\alpha\beta})
\end{aligned} \tag{49}$$

and the following properties:

$$\begin{aligned}
&\mathrm{d}V = \sqrt{g}\mathrm{d}\xi^1\,\mathrm{d}\xi^2\,\mathrm{d}\xi^3,\\
&\boldsymbol{n}_{(\alpha)}\mathrm{d}S = \boldsymbol{a}^{(\alpha)}\sqrt{g}\mathrm{d}\xi^\beta\,\mathrm{d}\xi^\gamma
\end{aligned} \tag{50}$$

with $\boldsymbol{a}^{(\alpha)}$ the contravariant basevector, perpendicular to the ξ^β and ξ^γ coordinate lines

$$\boldsymbol{a}_k^{(\alpha)} = \frac{\partial \xi^\alpha}{\partial x^k}. \tag{51}$$

Hence (48) becomes

$$\iiint_\Gamma \frac{\partial \rho}{\partial t}\sqrt{g}\mathrm{d}\xi^1\,\mathrm{d}\xi^2\,\mathrm{d}\xi^3 + \iint_{\partial\Gamma} \rho\boldsymbol{u}\cdot\boldsymbol{a}^{(\alpha)}\sqrt{g}\mathrm{d}\xi^\beta\,\mathrm{d}\xi^\gamma = 0, \tag{52}$$

$$\iiint_\Gamma \left(\frac{\partial \rho \boldsymbol{u}}{\partial t}\right)^{\diamondsuit}\sqrt{g}\mathrm{d}\xi^1\,\mathrm{d}\xi^2\,\mathrm{d}\xi^3 + \iint_{\partial\Gamma} p\boldsymbol{a}^{(\alpha)}\sqrt{g}\mathrm{d}\xi^\beta\,\mathrm{d}\xi^\gamma = 0, \tag{53}$$

$$\iiint_\Gamma \frac{\partial \rho}{\partial t}\sqrt{g}\mathrm{d}\xi^1\,\mathrm{d}\xi^2\,\mathrm{d}\xi^3 + \iiint_\Gamma \boldsymbol{u}\cdot\nabla\rho\sqrt{g}\mathrm{d}\xi^1\,\mathrm{d}\xi^2\,\mathrm{d}\xi^3 = \iiint_\Omega \mathrm{Cond}(\rho)\,\mathrm{d}V. \tag{54}$$

The gradient is transformed into

$$\nabla\phi = \frac{\partial\phi}{\partial\xi^\alpha}\boldsymbol{a}_\beta^{(\alpha)}\boldsymbol{a}_\beta^{(\gamma)}\boldsymbol{a}_{(\gamma)} = \frac{\partial\phi}{\partial\xi^\alpha}g^{\alpha\gamma}\boldsymbol{a}_{(\gamma)} = \frac{\partial\phi}{\partial\xi^\alpha}\boldsymbol{a}^{(\alpha)}. \tag{55}$$

Thus, Eq. (54) becomes

$$\iiint_{\Gamma} \frac{\partial \rho}{\partial t} \sqrt{g} \mathrm{d}\xi^1 \mathrm{d}\xi^2 \mathrm{d}\xi^3 + \iiint_{\Gamma} \boldsymbol{u} \cdot \frac{\partial \rho}{\partial \xi^\alpha} \boldsymbol{a}^{(\alpha)} \sqrt{g} \mathrm{d}\xi^1 \mathrm{d}\xi^2 \mathrm{d}\xi^3 = \iiint_{\Omega} \mathrm{Cond}(\rho) \mathrm{d}V. \tag{56}$$

The inner product $\boldsymbol{u} \cdot \boldsymbol{a}^{(\alpha)}$ equals, by definition, the contravariant component U^α of the velocity vector $\boldsymbol{u}$

$$U^\alpha = \boldsymbol{u} \cdot \boldsymbol{a}^{(\alpha)}. \tag{57}$$

It is known [10,16] that it is better to consider the contravariant fluxes V^α since they are continuous in the entire domain

$$V^\alpha = U^\alpha \sqrt{g}. \tag{58}$$

Eq. (52) then becomes

$$\iiint_{\Gamma} \frac{\partial \rho}{\partial t} \sqrt{g} \mathrm{d}\xi^1 \mathrm{d}\xi^2 \mathrm{d}\xi^3 + \iint_{\partial \Gamma} \rho V^\alpha \mathrm{d}\xi^\beta \mathrm{d}\xi^\gamma = 0, \tag{59}$$

while Eq. (56) reads

$$\iiint_{\Gamma} \frac{\partial \rho}{\partial t} \sqrt{g} \mathrm{d}\xi^1 \mathrm{d}\xi^2 \mathrm{d}\xi^3 + \iiint_{\Gamma} \frac{\partial \rho}{\partial \xi^\alpha} V^\alpha \mathrm{d}\xi^1 \mathrm{d}\xi^2 \mathrm{d}\xi^3 = \iiint_{\Omega} \mathrm{Cond}(\rho) \mathrm{d}V. \tag{60}$$

The finite volume formulation for the control volume around the node with index θ immediately follows:

$$|\Omega_\theta| \left(\frac{\partial \rho}{\partial t} \right)_\theta + \sum_\alpha [\rho V^\alpha]_{\partial \Gamma_{\theta_{\alpha-}}}^{\partial \Gamma_{\theta_{\alpha+}}} = 0, \tag{61}$$

$$|\Omega_\theta| \left(\frac{\partial \rho}{\partial t} \right)_\theta + \sum_\alpha (V^\alpha)_\theta [\rho]_{\partial \Gamma_{\theta_{\alpha-}}}^{\partial \Gamma_{\theta_{\alpha+}}} = \iiint_{\Omega} \mathrm{Cond}(\rho) \mathrm{d}V. \tag{62}$$

$\partial \Gamma_{\theta_{\alpha+}}$ indicates the part in the positive α-direction of the boundary face of the control volume around the node with index θ, so that the summation sums over all 6 faces of the control volume.

The momentum equation (53) can also be written in terms of the contravariant fluxes. Therefore the inner product of (53) and the contravariant basevector, averaged over the control volume, $\bar{\boldsymbol{a}}_\theta^{(\alpha)}$ is taken

$$\iiint_{\Gamma} \bar{\boldsymbol{a}}_\theta^{(\alpha)} \cdot \left(\frac{\partial \rho \boldsymbol{u}}{\partial t} \right)^{\diamondsuit} \sqrt{g} \mathrm{d}\xi^1 \mathrm{d}\xi^2 \mathrm{d}\xi^3 + \bar{\boldsymbol{a}}_\theta^{(\alpha)} \cdot \iint_{\partial \Gamma} p \boldsymbol{a}^{(\delta)} \sqrt{g} \mathrm{d}\xi^\beta \mathrm{d}\xi^\gamma = 0, \tag{63}$$

which gives in finite volume formulation

$$\left(\frac{\partial \rho V^\alpha}{\partial t} \right)_\theta^{\diamondsuit} + \bar{\boldsymbol{a}}_\theta^{(\alpha)} \cdot \sum_\delta \left[p \boldsymbol{a}^{(\delta)} \sqrt{g} \right]_{\partial \Gamma_{\theta_{\delta-}}}^{\partial \Gamma_{\theta_{\delta+}}} = 0. \tag{64}$$

4.2. Algorithm in general curvilinear coordinates

Since Eqs. (61), (62) and (64) are very similar to the original transport equation in one dimension, a flux correction term can be derived in the same fashion, provided that the derivation is done on the Cartesian coordinate system (ξ^1, ξ^2, ξ^3) with the contravariant flux vectors V^α as velocity unknowns. The only difficulty appears in the pressure term, which is now more complicated as can be seen in (64). We make abstraction of this pressure term by the definition

$$\mathcal{P}_\theta = \bar{\boldsymbol{a}}_\theta^{(\alpha)} \cdot \sum_\delta [p \boldsymbol{a}^{(\delta)} \sqrt{g}]_{\partial \Gamma_{\theta_{\delta-}}}^{\partial \Gamma_{\theta_{\delta+}}}. \tag{65}$$

Eqs. (26), (29), (32), (37), (39) and (45) become respectively

$$\frac{V_{\theta_{\alpha+}}^{\alpha^{n+1}} - \widetilde{V^{\alpha}}^{*}_{\theta_{\alpha+}}}{\Delta t} = -\frac{1}{\tilde{\rho}^{n+1}_{\theta_{\alpha+}}}\mathcal{P}_{\theta_{\alpha+}}, \tag{66}$$

$$\overline{V^{\alpha}}^{n+1}_{\theta} - \overline{\widetilde{V^{\alpha}}}^{*}_{\theta} = -\Delta t \frac{\overline{\mathcal{P}}}{\tilde{\rho}}\bigg|^{n+1}_{\theta}, \tag{67}$$

$$\begin{aligned}|\Omega_\theta|\left(\frac{\partial \rho}{\partial t}\right)_\theta &= -\sum_\alpha [\rho V^\alpha]^{\partial\Gamma_{\theta_{\alpha+}}}_{\partial\Gamma_{\theta_{\alpha-}}} \\ &= -\sum_\alpha [\rho^{n+1}_{\alpha R} V^{\alpha^{n+1}}_{\theta_{\alpha+}} - \rho^{n+1}_{\alpha L} V^{\alpha^{n+1}}_{\theta_{\alpha-}}] \\ &= -\sum_\alpha [\rho^{n+1}_{\alpha R} \widetilde{V^{\alpha}}^{*}_{\theta_{\alpha+}} - \rho^{n+1}_{\alpha L} \widetilde{V^{\alpha}}^{*}_{\theta_{\alpha-}}] + \Delta t \sum_\alpha \left[\rho^{n+1}_{\alpha R}\frac{\mathcal{P}}{\tilde{\rho}}\bigg|^{n+1}_{\theta_{\alpha+}} - \rho^{n+1}_{\alpha L}\frac{\mathcal{P}}{\tilde{\rho}}\bigg|^{n+1}_{\theta_{\alpha+}}\right],\end{aligned} \tag{68}$$

$$\varepsilon^{\alpha}_{\theta_{\alpha+}} = \left[\widetilde{V^{\alpha}}^{*}_{\theta_{\alpha+}} - \widetilde{\overline{V^{\alpha}}}^{*}_{\theta_{\alpha+}}\right] - \Delta t\left[\frac{\mathcal{P}}{\tilde{\rho}}\bigg|^{n+1}_{\theta_{\alpha+}} - \frac{\widetilde{\overline{\mathcal{P}}}}{\tilde{\rho}}\bigg|^{n+1}_{\theta_{\alpha+}}\right], \tag{69}$$

$$\hat{\varepsilon}^{\alpha}_{\theta_{\alpha+}} = -\Delta t\left[\frac{\mathcal{P}}{\tilde{\rho}}\bigg|^{n+1}_{\theta_{\alpha+}} - \frac{\widetilde{\overline{\mathcal{P}}}}{\tilde{\rho}}\bigg|^{n+1}_{\theta_{\alpha+}}\right], \tag{70}$$

$$\Delta t\left[\frac{\mathcal{P}}{\tilde{\rho}}\bigg|^{n+1}_{\theta_{\alpha+}} - \frac{\mathcal{P}}{\tilde{\rho}}\bigg|^{n+1}_{\theta_{\alpha-}}\right] = [\widetilde{V^{\alpha}}^{*}_{\theta_{\alpha}+} - \widetilde{V^{\alpha}}^{*}_{\theta_{\alpha-}}] - [Q^{\alpha^{n+1}}_{\theta_{\alpha+}} - Q^{\alpha^{n+1}}_{\theta_{\alpha-}}]. \tag{71}$$

In (71), Q denotes the discretized version of the heat flux, written in terms of ρ and evaluated at the cell faces. Using these equations, the algorithm is very similar to the one for cartesian coordinate systems (Fig. 2).

4.3. Remarks

4.3.1. Flux–velocity relation

The above equations consider the contravariant flux as primary variable. Since we are interested in the velocity itself in physical space, we apply the following conversion formulas:

$$V^{\alpha}_{\theta} = \iiint_{\Gamma} V^{\alpha}\mathrm{d}\xi^1\,\mathrm{d}\xi^2\,\mathrm{d}\xi^3 = \iiint_{\Gamma} \boldsymbol{a}^{(\alpha)}\cdot\boldsymbol{u}\sqrt{g}\mathrm{d}\xi^1\,\mathrm{d}\xi^2\,\mathrm{d}\xi^3 = \iiint_{\Omega} \boldsymbol{a}^{(\alpha)}\cdot\boldsymbol{u}\,\mathrm{d}V = \iiint_{\Omega} \boldsymbol{a}^{(\alpha)}\,\mathrm{d}V\cdot\boldsymbol{u}_\theta. \tag{72}$$

The inverse formula yields

$$\begin{aligned}u^{\alpha}_{\theta} &= \frac{1}{\Omega}\iiint_{\Omega} u^{\alpha}\,\mathrm{d}V = \frac{1}{\Omega}\iiint_{\Omega}\frac{\boldsymbol{a}_{(\alpha)}\cdot\boldsymbol{V}}{\sqrt{g}}\mathrm{d}V = \frac{1}{\Omega}\iiint_{\Gamma}\boldsymbol{a}_{(\alpha)}\cdot\boldsymbol{V}\mathrm{d}\xi^1\,\mathrm{d}\xi^2\,\mathrm{d}\xi^3 \\ &= \frac{1}{\Omega}\iiint_{\Gamma}\boldsymbol{a}_{(\alpha)}\mathrm{d}\xi^1\,\mathrm{d}\xi^2\,\mathrm{d}\xi^3\cdot\boldsymbol{V}_\theta.\end{aligned} \tag{73}$$

The integrals only contain geometrical quantities and can be exactly calculated.

Remark that the flux at the face is calculated as the average of the fluxes at the neighbouring nodes, which is not the same as calculating the flux from the face velocity, which would be the average of the neighbouring node velocities

$$V^{\alpha}_{\theta_{\alpha+}} = \frac{V^{\alpha}_{\theta_\alpha} + V^{\alpha}_{\theta_{\alpha++}}}{2} = \frac{1}{2}\left[\iiint_{\Omega_\theta}\boldsymbol{a}^{(\alpha)}\mathrm{d}V\cdot\boldsymbol{u}_\theta + \iiint_{\Omega_{\theta_{\alpha++}}}\boldsymbol{a}^{(\alpha)}\mathrm{d}V\cdot\boldsymbol{u}_{\theta_{\alpha++}}\right] \neq \iiint_{\Omega_{\theta_{\alpha+}}}\boldsymbol{a}^{(\alpha)}\mathrm{d}V\cdot\frac{\boldsymbol{u}_{\theta_\alpha}+\boldsymbol{u}_{\theta_{\alpha++}}}{2}. \tag{74}$$

4.3.2. Evaluation of $\mathcal{P}$

The evaluation of $\mathcal{P}$ is complicated but can be done in a straightforward manner. It is important to note that the evaluation at the surfaces of the term $p\boldsymbol{a}^{(\delta)}\sqrt{g}$ is well defined since the expression is continuous over the surface. Remark that here the exact geometrical quantity $\boldsymbol{a}^{(\delta)}\sqrt{g}$ can be used, integrated over the surface area, consistent with (63), from which this term originates.

5. Discussion: the failure of other cell-face velocity interpolations

5.1. The cure, seen from a different perspective

Let us reconsider the example of a 1D adiabatic channel (Section 2.3). The uncured algorithm results in a Laplacian-like operator with a stencil, clearly indicating the odd–even decoupling

$$\left[\begin{array}{ccccc} \frac{1}{\rho_{i-1}} & 0 & -\frac{1}{\rho_{i-1}}-\frac{1}{\rho_{i+1}} & 0 & \frac{1}{\rho_{i+1}} \end{array}\right]. \tag{75}$$

The adjusted algorithm, however, eliminates the spurious mode, resulting in a compact stencil

$$\left[\begin{array}{ccccc} 0 & \frac{1}{\rho_{i-\frac{1}{2}}} & -\frac{1}{\rho_{i-\frac{1}{2}}}-\frac{1}{\rho_{i+\frac{1}{2}}} & \frac{1}{\rho_{i+\frac{1}{2}}} & 0 \end{array}\right] \tag{76}$$

In constant density flows, the effect of the correction term $\hat{\varepsilon}$ can be visualized in stencil notation: by adding the correction term, the wide stencil is compacted [15,17]

$$\begin{array}{lccccc} & [& 1 & 0 & -2 & 0 & 1 &]_{\text{wide stencil}} \\ +[& -1 & 3 & -3 & 1 & 0 &]_{\hat{\varepsilon}\text{ on the left face}} \\ +[& 0 & 1 & -3 & 3 & -1 &]_{\hat{\varepsilon}\text{ on the right face}} \\ \hline =[& 0 & 4 & -8 & 4 & 0 &]_{\text{compact stencil}} \end{array}. \tag{77}$$

Consequently, adding the correction term to the non-cured constraining equation, results in the correct constraining equation. This observation does not hold in variable density flow. Indeed

$$\begin{array}{lccccc} [& \frac{1}{\rho_{i-1}} & 0 & -\frac{1}{\rho_{i-1}}-\frac{1}{\rho_{i+1}} & 0 & \frac{1}{\rho_{i+1}} &] \\ +[& -\frac{1}{\rho_{i-\frac{3}{2}}} & \frac{1}{\rho_{i-\frac{3}{2}}}+\frac{2}{\rho_{i-\frac{1}{2}}} & -\frac{2}{\rho_{i-\frac{1}{2}}}-\frac{1}{\rho_{i+\frac{1}{2}}} & \frac{1}{\rho_{i+\frac{1}{2}}} & 0 &] \\ +[& 0 & \frac{1}{\rho_{i-\frac{1}{2}}} & -\frac{1}{\rho_{i-\frac{1}{2}}}-\frac{2}{\rho_{i+\frac{1}{2}}} & \frac{2}{\rho_{i+\frac{1}{2}}}+\frac{1}{\rho_{i+\frac{3}{2}}} & -\frac{1}{\rho_{i+\frac{3}{2}}} &] \\ \hline \neq[& 0 & \frac{4}{\rho_{i-\frac{1}{2}}} & -\frac{4}{\rho_{i-\frac{1}{2}}}-\frac{4}{\rho_{i+\frac{1}{2}}} & \frac{4}{\rho_{i+\frac{1}{2}}} & 0 &] \end{array}. \tag{78}$$

The wide stencil, for which the above reasoning does hold, is

$$\left[\begin{array}{ccccc} \frac{1}{\rho_{i-\frac{3}{2}}} & -\frac{1}{\rho_{i-\frac{3}{2}}}+\frac{1}{\rho_{i-\frac{1}{2}}} & -\frac{1}{\rho_{i-\frac{1}{2}}}-\frac{1}{\rho_{i+\frac{1}{2}}} & \frac{1}{\rho_{i+\frac{1}{2}}}-\frac{1}{\rho_{i+\frac{3}{2}}} & \frac{1}{\rho_{i-\frac{3}{2}}} \end{array}\right] \tag{79}$$

which is hard to see a priori.

5.2. Demand for solvability

As explained in [17] for constant-density flows, the choice for the compacted Laplacian-like operator is arbitrary, as long as it is consistent. In variable density flows, where conductive effects enter, an extra condition (the solvability condition) appears. We have shown above that, using the present approach, we end up with a pressure equation which can be solved. To that purpose (as explained in Section 2.3) the conductive term requires a special discretization.

5.3. How to make other approaches work

From Section 5.1, we saw that (79) can be seen as the basic wide stencil. If we use the correction term $\hat{\varepsilon}$, as defined in (39), a regular compact stencil is obtained. If other cell-face velocity interpolations would have been used, a modified stencil for the poisson equation would be the result. In general, the correction terms take the following stencil, for the left and right face respectively:

$$\begin{aligned}&[a_1 \quad a_2 \quad a_3 \quad a_4 \quad 0],\\ &[0 \quad -b_1 \quad -b_2 \quad -b_3 \quad -b_4],\end{aligned} \tag{80}$$

where the coefficients must be chosen in such a way that the resulting expression for $\hat{\varepsilon}$ takes the form

$$\hat{\varepsilon}_{\mathrm{L}} = f\left(\left.\frac{\nabla p}{\rho}\right|_{i-\frac{3}{2}}, \left.\frac{\nabla p}{\rho}\right|_{i-\frac{1}{2}}, \left.\frac{\nabla p}{\rho}\right|_{i+\frac{1}{2}}\right). \tag{81}$$

The resulting '*compact*' stencil takes the form

$$\left[\frac{1}{\rho_{i-\frac{3}{2}}}+a_1 \quad -\frac{1}{\rho_{i-\frac{3}{2}}}+\frac{1}{\rho_{i-\frac{1}{2}}}+a_2+b_1 \quad -\frac{1}{\rho_{i-\frac{1}{2}}}-\frac{1}{\rho_{i+\frac{1}{2}}}+a_3+b_2 \quad \cdots \quad \frac{1}{\rho_{i+\frac{1}{2}}}-\frac{1}{\rho_{i+\frac{3}{2}}}+a_4+b_3 \quad \frac{1}{\rho_{i-\frac{3}{2}}}+b_4\right], \tag{82}$$

which can be written again as

$$\nabla u' = \mathcal{F}\left(\left.\frac{\nabla p}{\rho}\right|_{i-\frac{3}{2}}, \left.\frac{\nabla p}{\rho}\right|_{i-\frac{1}{2}}, \left.\frac{\nabla p}{\rho}\right|_{i+\frac{1}{2}}, \left.\frac{\nabla p}{\rho}\right|_{i+\frac{3}{2}}\right). \tag{83}$$

By this, the discretization of the conductive term is defined

$$\nabla q = \mathcal{F}\left(q_{i-\frac{3}{2}}, q_{i-\frac{1}{2}}, q_{i+\frac{1}{2}}, q_{i+\frac{3}{2}}\right). \tag{84}$$

5.4. Traps with other approaches

If other approaches are used, special requirements are needed for the discretization. In general, these requirements are not incorporated in the codes and the correction term for the cell-face velocity is seen merely as an ad hoc adjustment. There are however consequences involved. Some traps are listed:

- The correction term cannot be written as (81). Indeed: many used correction terms originate from constant density flow calculations, and even in variable density equations, the pressure Poisson equation is generally written as a constant coefficient Poisson equation, such that the constant density behavior is retained. If this condition is not fulfilled, it is not clear what a solvability condition should look like and an a priori discretization of the conductive terms cannot be determined.
- The conductive terms are not discretized properly. Since (84) can become complicated, it is tempting to take a simpler discretization for the conductive term. Unfortunately, the system becomes unsolvable, and elimination of one equation (to fix the pressure level) results in different solutions, depending on the equation eliminated.
- The compact stencil (76) is used, with a general correction term. Hence, the system is solvable (with normal discretization of the conductive terms), but the density stepping is no longer directly related to the constraining equation. As a result, properties of monotonicity or TVD, adherent the choice of the spatial discretization, are no longer guaranteed (if the continuity equation is used to calculate the density field), or mass is no longer conserved (if the density equation is used).

6. Application: thermally driven cavity

6.1. Problem description

We consider the flow in a differentially heated square cavity in which a temperature difference is applied to two opposite vertical walls, while the other sides of the square are perfectly thermally insulated (Fig. 4). Furthermore, large temperature differences are considered. For a variable density fluid, the Rayleigh number is defined as

$$Ra = \frac{g\rho_0^2(T_h - T_c)L^3 Pr}{T_0\mu_0^2}, \tag{85}$$

where L is the characteristic dimension of the cavity, T_h and T_c respectively the hot and cold temperatures applied to the vertical walls, T_0 a reference temperature equal to $(T_h + T_c)/2$, μ_0 a reference viscosity coefficient and ρ_0 a reference density, both corresponding to T_0. The gravitational constant is set to $g = 9.81\ \mathrm{m/s^2}$. The temperature difference can be presented by a non-dimensional parameter $\epsilon = (T_h - T_c)/(T_h + T_c)$. The heat transfer through the wall is represented by local Nusselt number

$$Nu(y) = \frac{Lk\partial T/\partial x|_{wall}}{k_0(T_h - T_c)} \tag{86}$$

and average Nusselt number

$$\overline{Nu} = \frac{1}{L}\int_{y=0}^{y=L} Nu(y)\mathrm{d}y. \tag{87}$$

In the above expressions $k_0 = k(T_0)$, $k(T)$ is the heat conduction coefficient $k(T) = \mu(T)C_p/Pr$. In the test cases considered here, the Prandtl number is assumed to remain constant, equal to $Pr = 0.71$, and the viscosity is given by Sutherland's law

$$\mu(T)/\mu^* = (T/T^*)^{3/2}(T^* + S)/(T + S) \tag{88}$$

with $T^* = 273$ K, $S = 110.5$ K, $\mu^* = 1.68 \times 10^{-5}$ kg/m/s, $C_p = \gamma R/(\gamma - 1)$, $\gamma = 1.4$ and $R = 287.0$ J/kg/K. The influence of the temperature on C_p is neglected. The problem is completely defined by the Rayleigh number, the value of ϵ, a reference state (here $p_0 = 101{,}325$ Pa, $T_0 = 600$ K, $\rho_0 = p_0/(RT_0)$), the previously mentioned fluid properties and the initial conditions.

Further details and benchmark studies can be found in [1,4,8,18–20].

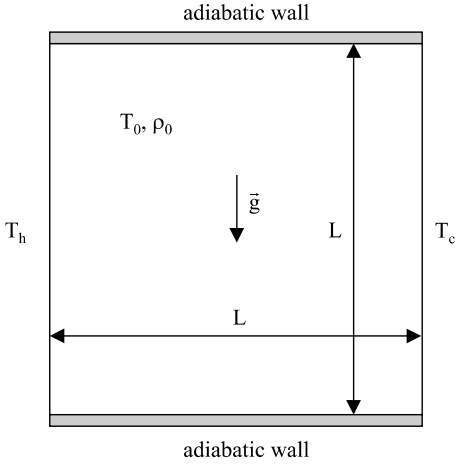

Fig. 4. Geometry, initial and boundary conditions for the thermally driven cavity problem

6.2. Implementation details

The general algorithm, as described in Section 4, is implemented on a cell-vertex colocated grid. A third-order Van Leer-κ method discretization is used for the convective fluxes and second-order central discretization for the diffusive fluxes and the pressure term. Because of the projection method, a special treatment of the boundaries is needed, and specific care must be taken for the temperature boundary condition at the isothermal walls. Since we are dealing with an enclosure, the total pressure p_0 is variable in time. To increase temporal accuracy, the pressure-correction algorithm is put in a multistage loop. Time stepping is done with the explicit form of a four stage Runge–Kutta scheme of a system $\frac{\partial \psi}{\partial t} = G(\psi)$

$$\begin{aligned}
\psi^{(0)} &= \psi^n, \\
\psi^{(1)*} &= \psi^{(0)} + \alpha_1 \Delta t G(\psi^{(0)}), \\
\psi^{(2)*} &= \psi^{(0)} + \alpha_2 \Delta t G(\psi^{(1)}), \\
\psi^{(3)*} &= \psi^{(0)} + \alpha_3 \Delta t G(\psi^{(2)}), \\
\psi^{(4)*} &= \psi^{(0)} + \alpha_4 \Delta t G(\psi^{(3)}), \\
\psi^{n+1} &= \psi^{(4)}.
\end{aligned} \tag{89}$$

Between every stage, the velocity field is corrected in order to obey the velocity constraint.

6.2.1. Boundary conditions

In general, zero flux boundary conditions are applied at walls: zero mass flux at all walls, and zero conductive flux at the adiabatic walls. Special care is needed for the boundary conditions of the predicted velocities at all walls and the temperature (read: density) at the isothermal walls. The correction term $\hat{\varepsilon}$ also has a special formulation at the boundaries.

6.2.1.1. Boundary conditions for u^*. We distinguish between the normal and tangential components of the predicted velocity vector $\vec{u}^* = \vec{u}^*_{\mathrm{n}} + \vec{u}^*_{\mathrm{t}}$. Because of the viscous forces, the tangential component $\vec{u}^*_{\mathrm{t}} = 0$. The normal component $\vec{u}^*_{\mathrm{n}}$, however, cannot be set to zero at the wall, since the 'blocking' effect of the wall on the flow field appears in the normal momentum equation under the form of a pressure force acting on the flow. Since in the operator splitting approach, the pressure terms are removed from the predictor momentum equations, the normal wall effect is removed as well, and no normal boundary conditions apply. For the corrected velocity, the opposed wall boundary conditions apply: the normal velocity component is set to zero, whereas the tangential component is left free.

6.2.1.2. Special treatment of the correction term at the boundaries. We recall expression (39) for $\hat{\varepsilon}$ for a 1D flow and evaluate this at the boundary, for node $i = 0$, starting from (35)

$$\begin{aligned}
&\rho_{\mathrm{R}}^{n+1} \tilde{u}^*_{\frac{1}{2}} - \Delta t \rho_{\mathrm{R}}^{n+1} \left.\frac{\nabla p}{\tilde{\rho}}\right|^{n+1}_{\frac{1}{2}} = \rho_{\mathrm{R}}^{n+1} \underline{u}^{n+1}_{\frac{1}{2}}, \\
&(38) \underset{\Longleftrightarrow}{\text{with } u_0 = 0} \quad \frac{u_0^* + u_1^*}{2} - \Delta t \left.\frac{\nabla p}{\tilde{\rho}}\right|^{n+1}_{\frac{1}{2}} = \frac{1}{2} u_1^{n+1} + \hat{\varepsilon}_{\frac{1}{2}}, \\
&(30) \underset{\Longleftrightarrow}{} \quad \frac{u_0^* + u_1^*}{2} - \Delta t \left.\frac{\nabla p}{\tilde{\rho}}\right|^{n+1}_{\frac{1}{2}} = \frac{1}{2} u_1^* - \Delta t \frac{1}{2} \left.\frac{\overline{\nabla p}}{\tilde{\rho}}\right|^{n+1}_{1} + \hat{\varepsilon}_{\frac{1}{2}},
\end{aligned} \tag{90}$$

so that the correction term at the boundaries becomes

$$\hat{\varepsilon}_{\frac{1}{2}} = -\Delta t \left[\left.\frac{\nabla p}{\tilde{\rho}}\right|^{n+1}_{\frac{1}{2}} - \frac{1}{2} \left.\frac{\overline{\nabla p}}{\tilde{\rho}}\right|^{n+1}_{1} \right] + \frac{u_0^*}{2}. \tag{91}$$

6.2.1.3. Boundary conditions at isothermal walls. A peculiarity of the present pressure-correction formulation is that a density stepping is used instead of the commonly applied temperature stepping. As a consequence, the Dirichlet boundary condition for temperature cannot directly be enforced. This problem is solved in the following way. The requirement $\frac{\partial T}{\partial t} = 0$ gives

$$\begin{aligned} &\frac{T^{n+1} - T^n}{\Delta t} = 0, \\ &\iff \frac{1}{\Delta t}\left(\frac{p_0^{n+1}}{\rho^{n+1}} - \frac{p_0^n}{\rho^n}\right) = 0, \\ &\iff \frac{p_0^n}{\rho^n \rho^{n+1}} \frac{\rho^n - \rho^{n+1}}{\Delta t} + \frac{1}{\rho^{n+1}} \frac{p_0^{n+1} - p_0^n}{\Delta t} = 0. \end{aligned} \tag{92}$$

At the boundary, $\frac{\partial \rho}{\partial t}$ can be expressed by Eq. (2), with $u_i = 0$

$$\begin{aligned} &\frac{\rho^{n+1} - \rho^n}{\Delta t} = -\frac{\rho_{\mathrm{R}}^n u_{i+\frac{1}{2}}^n}{\Delta x} \quad \text{for } i = 0, \\ &\frac{\rho^{n+1} - \rho^n}{\Delta t} = \frac{\rho_{\mathrm{L}}^n u_{i-\frac{1}{2}}^n}{\Delta x} \quad \text{for } i = N. \end{aligned} \tag{93}$$

The last expression can be used to formulate the constraint for the velocity field at these nodes. For an internal node, the constraint follows from elimination of $\frac{\partial \rho}{\partial t}$ from (2) and (8), yielding

$$\frac{\partial u_i^n}{\partial x_i} = -\frac{1}{\gamma p_0^n} \frac{\mathrm{d}p_0}{\mathrm{d}t} + \frac{\partial q_i^n}{\partial x_i}. \tag{94}$$

Inserting (93) into (92), yields the constraint at the isothermal boundary nodes (e.g. for node $i = 0$)

$$\frac{\partial u_i^n}{\partial x_i} = -\frac{\rho^n}{\rho_{\mathrm{R}}^n} \frac{1}{p_0^n} \frac{\mathrm{d}p_0}{\mathrm{d}t} \tag{95}$$

from which the pressure equation follows. There is, however, a small difficulty with the previous expression: since we do not know the direction of the velocity u^n, the exact extrapolations ρ_{R}^n and ρ_{L}^n cannot yet be determined. The solution is found in the following identity for enclosures:

$$\int_V \frac{\partial u_i^n}{\partial x_i} \mathrm{d}V \equiv \oint_{\partial V} \vec{u} \cdot \mathrm{d}\vec{S} = 0. \tag{96}$$

In finite volume formulation, we then obtain

$$\begin{aligned} \int_V \frac{\partial u_i^n}{\partial x_i} \mathrm{d}V &= \sum_{\text{internal nodes}} \frac{\partial u_k^n}{\partial x_k} V_i + \sum_{\text{isothermal wall}} \frac{\partial u_k^n}{\partial x_k} V_i \iff 0 \\ &= -\frac{1}{\gamma p_0^n} \frac{\mathrm{d}p_0}{\mathrm{d}t} \underbrace{\left[\sum\nolimits_{\text{internal nodes}} V_i + \sum\nolimits_{\text{isothermal wall}} \frac{\gamma \rho^n}{\rho_{R/L}^n} V_i\right]}_{\mathcal{V} \geqslant 0} + \sum_{\text{internal nodes}} \frac{\partial q_k^n}{\partial x_k} V_i \end{aligned} \tag{97}$$

from which the sign of $\frac{\mathrm{d}p_0}{\mathrm{d}t}$ can be determined, and, because of (95), the sign of $\frac{\partial u_i^n}{\partial x_i}$, such that the exact extrapolation for ρ is known. Because of that, term $\mathcal{V}$ in expression (97) is known, and $\frac{\mathrm{d}p_0}{\mathrm{d}t} = \frac{p_0^{n+1} - p_0^n}{\Delta t}$ can be calculated.

The above 1D reasoning is easily extended to higher dimensions, if we assume that no transport occurs parallel to the wall at the isothermal boundary nodes.

6.2.2. Time step restriction

For a one-dimensional problem, using a forward Euler scheme, the time step restriction is given by the semi-empirical stability condition

$$\Delta t \leqslant \frac{1}{\frac{1}{(\Delta t)_{\mathrm{c}}} + \frac{1}{(\Delta t)_{\mathrm{d}}}} \tag{98}$$

with

$$(\Delta t)_c \leqslant \frac{\Delta x}{\frac{1}{2}\left(\underline{u}_{i-\frac{1}{2}} + \underline{u}_{i+\frac{1}{2}}\right)}, \tag{99}$$

and

$$(\Delta t)_d \leqslant \frac{2\Delta x^2}{(\rho_L + \rho_R)\left(\tilde{k}_{i-\frac{1}{2}} + \tilde{k}_{i+\frac{1}{2}}\right)} \tag{100}$$

with $\tilde{k}_{i+\frac{1}{2}} = \frac{\kappa_{i+\frac{1}{2}}}{Re_\infty Pr_\infty \rho_i \rho_{i+1}}$.

When $Pr_\infty < 1$, the viscous time step limit is less restringent than the conductive time step limit, so that stability for the momentum equation is also ensured.

6.3. Results

For a non-dimensional temperature difference $\epsilon = 0.6$, cases with four different Rayleigh numbers ($Ra = 10^3$, 10^4, 10^5 and 10^6) are calculated. A uniform grid with square control volumes on a 64×64 mesh

Table 1
Nusselt number at the midplane and mean pressure for different Rayleigh numbers on a 64×64 mesh

Ra	$\overline{Nu}$	$\bar{p}/P_0$	$\overline{Nu}$ [19]	$\bar{p}/P_0$ [19]
10^3	1.1061	0.9381	1.1077	0.93805
10^4	2.2115	0.9166	2.218	0.91463
10^5	4.4333	0.9293	4.480	0.92196
10^6	8.3747	0.9487	8.687	0.92449

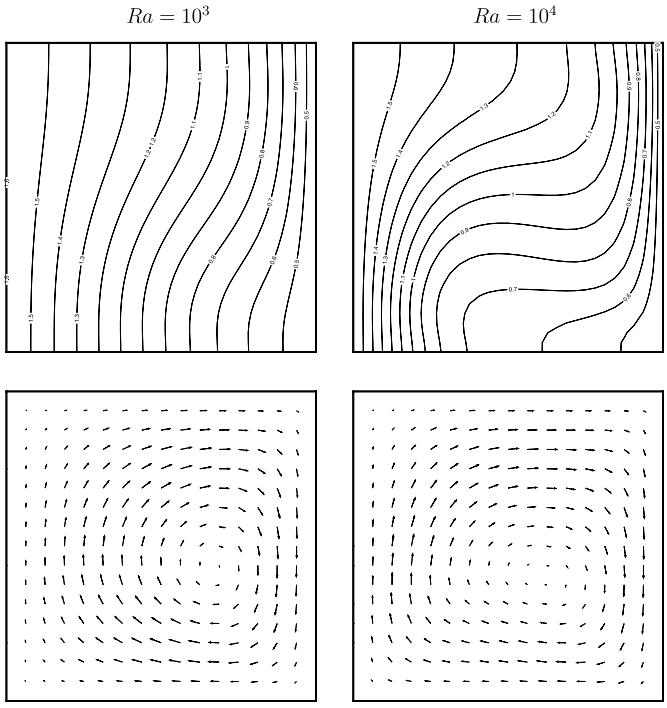

Fig. 5. Isolines for the dimensionless temperature ϵ (upper) and velocity vector-fields (lower) for $Ra = 10^3$ (left) and 10^4 (right). Isolines for the temperature range from $\epsilon = -0.6$ to $\epsilon = 0.6$ with intervals of 0.1. Velocity vectors are scaled with the maximum velocity in the domain.

is used. According to the stability domain of the multistage algorithm (89), with coefficients $\left\{\frac{1}{4},\frac{1}{3},\frac{1}{2},1\right\}$, the time step is set to 1.5 times the maximum timestep as defined in Eq. (98).

The results are summarized in Table 1. The mean pressure is given by p_0. The Nusselt number is evaluated at the midplane between the two isothermal walls. Comparison with the data obtained in [19] for the full Navier–Stokes equations shows good agreement for lower Rayleigh numbers. For the higher Rayleigh numbers, there is a larger error, which is due to the relative coarse grid used for these calculations (for comparison a calculation of $Ra = 10^6$ on a 128×128 mesh yields $\overline{Nu} = 8.6880$ and $\bar{p}/P_0 = 0.9307$). Qualitatively, good results were obtained for all Rayleigh numbers, as can be seen in the isotemperature lines and velocity fields (Figs. 5 and 6). The temperature and velocity fields are smooth, even when relative coarse meshes are used, where the odd–even decoupling is expected to be more pronounced [3].

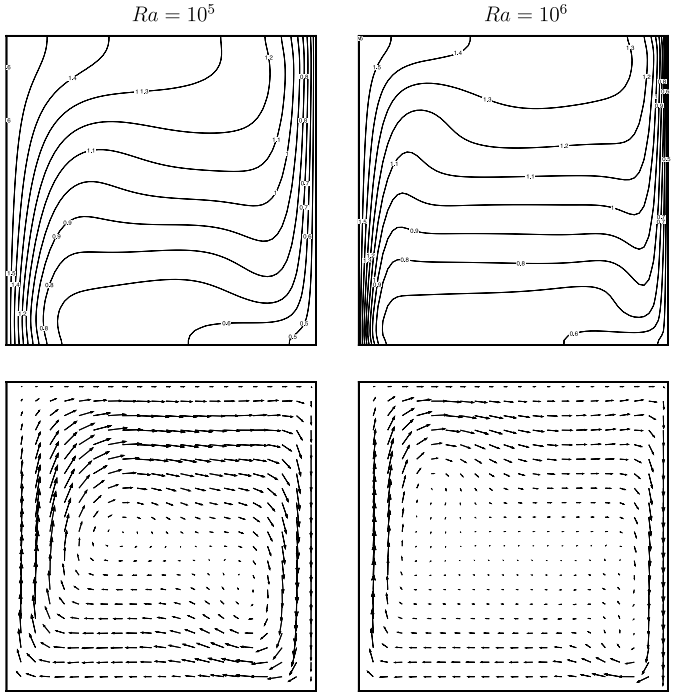

Fig. 6. Isolines for the dimensionless temperature ϵ (upper) and velocity vector-fields (lower) for $Ra = 10^5$(left) and 10^6(right). Isolines for the temperature range from $\epsilon = -0.6$ to $\epsilon = 0.6$ with intervals of 0.1. Velocity vectors are scaled with the maximum velocity in the domain.

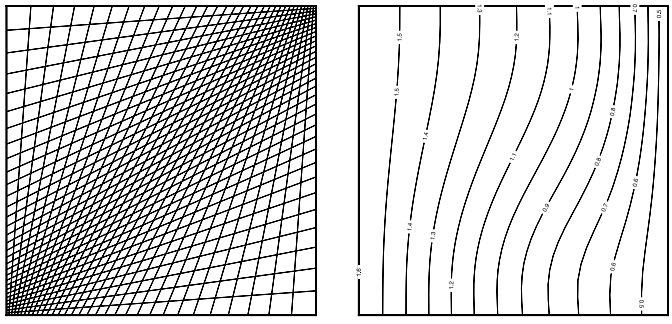

Fig. 7. 32×32 highly stretched and skewed grid (left), resulting in smooth isolines for the dimensionless temperature ϵ for $Ra = 10^3$(right).

Table 2
Nusselt number at the cold wall and mean pressure for $Ra = 10^3$

Cartesian		Stretched	
$\overline{Nu}_{\text{cold}}$	$\bar{p}/P_0$	$\overline{Nu}_{\text{cold}}$	$\bar{p}/P_0$
1.1080	0.9383	1.081	0.9406

Comparison between cartesian and stretched grid of 32×32 nodes.

The behavior of the algorithm on highly stretched and skewed grids is checked as well. As an example, the resulting temperature field for $Ra = 10^3$ on a 32×32 non-uniform grid is shown in Fig. 7, resulting in practically the same solution as on the cartesian grid (Table 2), without odd–even decoupling.

7. Conclusions

A solution was presented for the odd–even decoupling of the pressure field in the framework of pressure-correction algorithms for variable density flow. It consists of two remedies. First, a correction term for the cell-face velocity, similar to the proposition in [15] is introduced (Eq. (37)). Secondly, the wide stencil for the discrete Laplacian is compacted, involving only the immediate neighbours of the node and the node itself. It is important that the correction term does not appear in the pressure Poisson-like equation (Eq. (45)).

There is an additional advantage in the pressure equation (45) in terms of efficiency due to the absence of upwind density values. As a result, the Laplacian-like operator L needs to be evaluated only once each time step.

Finally, the method has been extended for three-dimensional curvilinear grids.

The algorithm is validated on the test case of a two-dimensional thermally driven cavity. The results are comparable to previous calculations. Even for highly stretched and skewed meshes, good results are obtained, showing the large applicability of the presented cure for odd–even decoupling.

Appendix A. Discretization of the conductive fluxes

We start from the semi-discretized equation (19), from which the velocity field in a 1D enclosure is derived

$$-\frac{\rho_R u_{i+\frac{1}{2}} - \rho_L u_{i-\frac{1}{2}}}{\Delta x} + u_i \frac{\rho_R - \rho_L}{\Delta x} = -\rho \frac{\partial q}{\partial x}, \tag{A.1}$$

where the cell-face velocities are defined as $u_{i+\frac{1}{2}} = (u_i + u_{i+1})/2$. We consider adiabatic walls at both ends.

A fully discretized version of (A.1) can formally be written in system notation as

$$DU = D'Q \iff LP = -DU^* - D'Q \tag{A.2}$$

with $U = [u_1 \quad u_2 \quad \cdots \quad u_N]^T$ the velocity vector, $Q = [q_1 \quad q_2 \quad \cdots \quad q_N]^T$ the conductive flux vector and D and D' discrete divergence operators, $L = DG$ the discrete Laplacian and G the discrete gradient operator. In all of the operators, extrapolated values for the density can be found.

The system is singular and contains a nullspace of dimension 2, for which $LP = 0$, based on the two pressure vectors $P_H = [1 \quad 1 \quad \cdots \quad 1]^T$ and $P_\pi = [1 \quad -1 \quad \cdots \quad (-1)^{N+1}]^T$. The same holds for the transpose of the operator L, resulting again in a nullspace of dimension 2, based on 2 vectors R_H and R_π, for which $R^T L = 0$.

(A.2) should be solvable for any choice of U^* and Q. For now, we are not interested in divergence operator D, so we choose $U^* = 0$. Requiring (A.2) to be solvable, yields following solvability conditions:

$$\begin{aligned} &R_\pi LP = 0 = -R_\pi D'Q \quad \text{and} \\ &R_H LP = 0 = -R_H D'Q \quad \forall Q \in \mathbb{R}^N. \end{aligned} \tag{A.3}$$

The discrete divergence operator D' must thus have a nullspace of dimension 2, based on the two basis vectors R_π and R_H. Since these two basisvectors cannot easily be determined, and strongly depend on the extrapolated

values of the density, the most obvious (and least computationally intensive) choice for the system to be solvable is $D' = D$. The fully discretized equation of (A.1) then becomes

$$-\frac{\rho_R u_{i+\frac{1}{2}} - \rho_L u_{i-\frac{1}{2}}}{\Delta x} + u_i \frac{\rho_R - \rho_L}{\Delta x} = -\frac{\rho_R q_{i+\frac{1}{2}} - \rho_L q_{i-\frac{1}{2}}}{\Delta x} + q_i \frac{\rho_R - \rho_L}{\Delta x} \tag{A.4}$$

with $q_{i+\frac{1}{2}} = (q_i + q_{i+1})/2$.

If the equation is discretized as (A.4), it is trivial to see that the system is solvable. Indeed: a solution exists and is found to be $u_i = q_i + \alpha_1(P_H)_i + \alpha_2(P_\pi)_i$, with $\alpha_l \in \mathbb{R},\ l = 1, 2$.

References

[1] D.R. Chenoweth, S. Paolucci, Natural convection in an enclosed vertical air layer with large horizontal temperature differences, Journal of Fluid Mechanics 169 (1986) 173–210.

[2] A.W. Date, Solution of Navier–Stokes equations on non-staggered grids, International Journal of Heat and Mass Transfer 36 (7) (1993) 1913–1922.

[3] A.W. Date, Fluid dynamical view of pressure checkerboarding problem and smoothing pressure correction on meshes with colocated variables, International Journal of Heat and Mass Transfer 46 (25) (2003) 4885–4898.

[4] G. De Vahl Davis, I.P. Jones, Natural convection in a square cavity, a comparison exercise, International Journal for Numerical Methods in Fluids 3 (1983) 249–264.

[5] E. Dick, A flux-vector splitting method for steady Navier–Stokes equations, International Journal for Numerical Methods in Fluids 9 (1988) 113–120.

[6] J.R. Edwards, M.S. Liou, Low diffusion flux-splitting methods for flows at all speeds, AIAA Journal 36 (1998) 1610–1617.

[7] F.H. Harlow, J.E. Welch, Numerical calculation of time-dependent viscous incompressible flow of fluid with a free surface, The Physics of Fluids 8 (1965) 2182–2189.

[8] P. Le Quéré, Accurate solutions to the square thermally driven cavity at high Rayleigh number, Computers & Fluids 20 (1991) 29–41.

[9] K. Nerinckx, J. Vierendeels, E. Dick, Mach uniformity through the coupled pressure and temperature correction algorithm, Journal of Computational Physics 206 (2005) 597–623.

[10] C.W. Oosterlee, P. Wesseling, A robust multigrid method for a discretization of the incompressible Navier–Stokes equations in general coordinates, Impact of Computing in Science and Engineering 5 (1993) 128–151.

[11] S.V. Patankar, D.B. Spalding, A calculation procedure for heat and mass transfer in three-dimensional parabolic flows, International Journal of Heat and Mass Transfer 15 (1972) 1787–1806.

[12] S. Paolucci, On the filtering of sound from the Navier–Stokes equations, Sandia National Laboratories report, SAND82-8257, 1982.

[13] M. Perić, R. Kessler, G. Scheuerer, Comparison of finite-volume numerical methods with staggered and colocated grids, Computers & Fluids 16 (4) (1988) 389–403.

[14] P. Rauwoens, K. Nerinckx, J. Vierendeels, E. Dick, B. Merci, A stable pressure-correction algorithm for low-speed turbulent combustion simulations, in: ECCOMAS CFD, 2006.

[15] C.M. Rhie, W.L. Chow, Numerical study of the turbulent flow past an isolated airfoil with trailing edge separation, AIAA Journal 21 (11) (1982) 1525–1532.

[16] A. Segal, P. Wesseling, J. Van Kan, C.W. Oosterlee, K. Kassels, Invariant discretization of the incompressible Navier–Stokes equations in boundary fitted coordinates, International Journal for Numerical Methods in Fluids 15 (1992) 411–426.

[17] D. Tafti, Alternate formulations for the pressure equation Laplacian on a collocated grid for solving the unsteady incompressible Navier–Stokes equations, Journal of Computational Physics 116 (1995) 143–453.

[18] J. Vierendeels, K. Riemslagh, E. Dick, A multigrid semi-implicit line-method for viscous incompressible and low-Mach-number flows on high aspect ratio grids, Journal of Computational Physics 154 (1999) 310–341.

[19] J. Vierendeels, B. Merci, E. Dick, Benchmark solutions for the natural convective heat transfer problem in a square cavity with large horizontal temperature differences, International Journal of Numerical Methods for Heat & Fluid Flow 13 (8) (2003) 1057–1078.

[20] J. Vierendeels, B. Merci, E. Dick, A multigrid method for natural convective heat transfer with large temperature differences, Journal of Computational and Applied Mathematics 168 (2004) 509–517.